2013-05-03

Signatures of Dynamic Screening in Interfacial Thermal Transport of Graphene

UTD AUTHOR(S): Zhun-Yong Ong and Massimo V. Fischetti

Signatures of dynamic screening in interfacial thermal transport of graphene

Zhun-Yong Ong,[1,*] Massimo V. Fischetti,[1] Andrey Y. Serov,[2,3] and Eric Pop[2,3,4,†]

[1]*Department of Materials Science & Engineering, University of Texas at Dallas RL10, Texas 75080, USA*

[2]*Department of Electrical & Computer Engineering, University of Illinois, Urbana-Champaign, Urbana, Illinois 61801, USA*

[3]*Micro and Nanotechnology Lab, University of Illinois, Urbana-Champaign, Illinois 61801, USA*

[4]*Beckman Institute of Advanced Science and Technology, University of Illinois, Urbana-Champaign, Illinois 61801, USA*

(Received 1 February 2013; published 3 May 2013)

The interaction between graphene and various substrates plays an important and limiting role on the behavior of graphene films and devices. Here we uncover that dynamic screening of so-called remote substrate phonons (RPs) has a significant effect on the thermal coupling at the graphene-substrate interface. We calculate the thermal conductance h_{RP} between graphene electrons and substrate, and its dependence on carrier density and temperature for SiO_2, HfO_2, h-BN, and Al_2O_3 substrates. The dynamic screening of RPs leads to one order of magnitude or more decrease in h_{RP} and a change in its dependence on carrier density. Dynamic screening predicts a decrease of $\sim$1 MW K^{-1} m^{-2} while static screening predicts a rise of $\sim$10 MW K^{-1} m^{-2} when the carrier density in Al_2O_3-supported graphene is increased from 10^{12} to 10^{13} cm^{-2}.

DOI: 10.1103/PhysRevB.87.195404 PACS number(s): 65.80.Ck, 68.47.Gh, 72.80.Vp, 79.60.Jv

Insulating materials such as SiO_2 and HfO_2 are typically used as substrates and gate dielectric for graphene electronics. However, supported graphene[1] is known to have a reduced carrier mobility compared to suspended single-layer graphene (SLG).[2,3] This degradation in electrical transport behavior is due to the scattering of electrons by impurities in the substrate as well as by the surface excitations, commonly believed to be surface polar phonons (SPP),[4] which are characteristic of polar dielectrics like SiO_2. Although interaction with surface excitations has been recognized as an important limiting factor in electron transport,[5,6] its role in thermal energy exchange between SLG and the substrate has not been systematically studied.

Admittedly, heat dissipation is not a significant consideration at low-field transport (e.g., <0.1 V/μm) in graphene field-effect transistors (GFETs); however most practical applications call for large currents which lead to Joule heating,[7,8] with heat dissipation from the graphene to the substrate playing an important role in device performance.[9] With increasing miniaturization and higher current densities (especially in radio-frequency applications[10]), managing power dissipation has become a significant problem in nanoelectronics.[9] To manage heat dissipation more efficiently, a better understanding of interfacial thermal transport between materials is needed. One of the principal channels for interfacial thermal transport is vibrational (phonon-phonon) coupling,[11] while coupling with surface polar excitations is another; their contributions to the total thermal boundary conductance (TBC) are h_{ph} and h_{RP}, respectively. Assuming that the two heat dissipation channels are additive, the Kapitza conductance h is their sum, i.e., $h = h_{ph} + h_{RP}$. Typical h values for the carbon-substrate interface are in the range of 20 to 200 MW K^{-1} m^{-2}.[12–16] The electronic contribution to the Kapitza conductance of bulk metal-insulator interfaces has been estimated to be negligible[17]; however the relative contributions of h_{ph} and h_{RP} could be very different in monolayer materials like graphene, where all electrons are in intimate proximity to the substrate. Energy dissipation via vibrational coupling[13,18,19] and electron-SPP scattering[20] has been explored in carbon nanotubes. Rotkin and co-workers[20] estimate that h_{RP} is comparable to h_{ph} in CNTs on SiO_2. These results suggest that the energy transfer rate through surface polar excitations may be varied by modulating the graphene carrier density through a gate voltage. This offers the intriguing possibility of controlling interfacial heat transfer between graphene and the substrate.

In a polar dielectric like SiO_2, the substrate dipoles create an oscillating electric field which extends outwards and decays exponentially with distance from the surface.[21] The surface excitations from this field interact with the SLG that lies some distance ($\sim$0.2 to 1 nm) above the substrate (hence the term "remote phonon") and scatters the graphene electrons inelastically, leading to momentum and energy exchange. The effect of these surface excitations on electron mobility in graphene has been investigated in several works in recent years,[4–6,22] but the consequence of this coupling with respect to heat transfer has not been explored to the same extent.[23,24] Furthermore, the nature of the excitations used has not been consistent, with some studies assuming them to be bare SPPs[24] and others SPPs with static screening.[23] Given the plethora of scattering mechanisms in electron transport, the electrical transport measurements cannot be used to probe the effect of screening on remote phonon scattering. On the other hand, only remote phonon scattering leads to direct energy exchange between the SLG and the substrate. Thus, Kapitza conductance measurements can be used to investigate the phenomenon of dynamic screening in remote phonon scattering. It is also possible for energy to be transferred from the SLG to the substrate *indirectly*. For example, the electron can emit an intrinsic acoustic or optical phonon which leads to an increase in the SLG lattice temperature. This lattice temperature rise is dissipated to the substrate via vibrational coupling between the SLG and the substrate. The first figure of Ref. 23 gives a detailed schematic of the different cooling pathways of hot electrons in supported graphene.

Experiments have also shown that the surface excitations of supported graphene are different from bare SPP excitations.[25,26] Using infrared nanoscopy, Fei and

co-workers[25] found that graphene plasmons couple strongly to the SiO_2 surface optical (SO) phonons. Angle-resolved reflection electron-energy-loss spectroscopic (AREELS) measurements by Liu and Willis[26] also suggest strong coupling between graphene plasmons and SO phonons. These experimental measurements provide compelling evidence that the substrate surface excitations are not pure SPP modes but excitations formed from the hybridization of the graphene plasmons and SPPs. Two of us (Ong and Fischetti) have recently formulated a theory of interfacial plasmon-phonons (IPPs) in SLG to describe this hybridization phenomenon in which the IPPs can be interpreted as dynamically screened SPPs.[27,28] The full details of the theory will not be presented here as it is outside the scope of the paper. Instead, we make use of the final results of the theory, i.e., the IPP dispersion and electron-IPP coupling coefficients, to compute the heat transfer coefficient.

I. THERMAL BOUNDARY CONDUCTANCE (TBC)

In this section we derive the thermal conductance between the electrons and the remote phonons (RPs) from the energy relaxation rate of electrons scattering with the RPs. The equation for the rate of change in the Bose-Einstein (BE) occupation of the γ branch phonon mode N_q^γ at $\mathbf{q}$ is

$$\frac{dN_{\gamma,\mathbf{q}}}{dt} = -g_s g_v \sum_{\mathbf{p}} \left(W^{(\mathrm{abs})}_{s,\mathbf{p}\to s',\mathbf{p}+\mathbf{q}} - W^{(\mathrm{ems})}_{s,\mathbf{p}\to s',\mathbf{p}-\mathbf{q}}\right), \quad (1)$$

where g_s and g_v are the spin and valley degeneracy, respectively, in SLG. $W^{(\mathrm{abs})}_{s,\mathbf{p}\to s',\mathbf{p}+\mathbf{q}}$ ($W^{(\mathrm{ems})}_{s,\mathbf{p}\to s',\mathbf{p}-\mathbf{q}}$) is the rate of absorption (emission) of a $(\gamma,\mathbf{q})$ phonon by an electron making the transition from the initial state in band s (=1 for conduction and −1 for valence) at wave vector $\mathbf{p}$ to the final state in band s' at wave vector $\mathbf{p}+\mathbf{q}$ ($\mathbf{p}-\mathbf{q}$). The absorption (emission) rate is explicitly given by

$$\begin{pmatrix} W^{(\mathrm{abs})}_{s,\mathbf{p}\to s',\mathbf{p}+\mathbf{q}} \\ W^{(\mathrm{ems})}_{s,\mathbf{p}\to s',\mathbf{p}-\mathbf{q}} \end{pmatrix} = \frac{2\pi}{\hbar}\left|M^\gamma_{\mathbf{q}}\right|^2 \times \begin{pmatrix} \left|\alpha^{ss'}_{\mathbf{p}+\mathbf{q},\mathbf{p}}\right|^2 F^{ss'}_{\mathbf{p},\mathbf{p}+\mathbf{q}} N_{\gamma,\mathbf{q}}\delta\left(E^{s'}_{\mathbf{p}+\mathbf{q}} - E^s_{\mathbf{p}} - \hbar\omega^\gamma_{\mathbf{q}}\right) \\ \left|\alpha^{ss'}_{\mathbf{p}-\mathbf{q},\mathbf{p}}\right|^2 F^{ss'}_{\mathbf{p},\mathbf{p}-\mathbf{q}} (N_{\gamma,\mathbf{q}}+1)\delta\left(E^{s'}_{\mathbf{p}-\mathbf{q}} - E^s_{\mathbf{p}} + \hbar\omega^\gamma_{\mathbf{q}}\right) \end{pmatrix},$$

where $F^{ss'}_{\mathbf{p},\mathbf{q}} = f^s_{\mathbf{p}}\left(1 - f^{s'}_{\mathbf{q}}\right)$ and $M^\gamma_{\mathbf{q}}$, $\alpha^{ss'}_{\mathbf{k},\mathbf{p}}$, $f^s_{\mathbf{p}}$, and $E^s_{\mathbf{p}} = s\hbar v_F|\mathbf{p}|$ are the electron-phonon coupling coefficient, the overlap integral, the Fermi-Dirac (FD) occupation, and eigenenergy of the of the $(s,\mathbf{p})$ electron state, respectively. After some algebra, we write the sum of the absorption (emission) terms compactly as

$$\sum_{\mathbf{p}ss'} \begin{pmatrix} W^{(\mathrm{abs})}_{s,\mathbf{p}\to s',\mathbf{p}+\mathbf{q}} \\ W^{(\mathrm{ems})}_{s,\mathbf{p}\to s',\mathbf{p}-\mathbf{q}} \end{pmatrix} = \frac{2\pi\Omega}{g_s g_v \hbar}\left|M^\gamma_{\mathbf{q}}\right|^2 \begin{pmatrix} N_{\gamma,\mathbf{q}} S_0\left(\mathbf{q},\omega^\gamma_{\mathbf{q}}\right) \\ (N_{\gamma,\mathbf{q}}+1) S_0\left(-\mathbf{q},-\omega^\gamma_{\mathbf{q}}\right) \end{pmatrix},$$

where $S_o(\mathbf{q},\omega)$ is the *dynamic structure factor*[29,30] of SLG and can be written explicitly as

$$S_o(\mathbf{q},\omega) = \frac{g_s g_v}{\Omega}\sum_{\mathbf{p}ss'}\left|\alpha^{ss'}_{\mathbf{p}+\mathbf{q},\mathbf{p}}\right|^2 F^{ss'}_{\mathbf{p},\mathbf{p}+\mathbf{q}}\delta\left(E^{s'}_{\mathbf{p}+\mathbf{q}} - E^s_{\mathbf{p}} - \hbar\omega\right),$$

and Ω is the interfacial area. Using the relationship $S_0(\mathbf{q},\omega) = e^{\beta\hbar\omega}S_0(-\mathbf{q},-\omega)$, Eq. (1) simplifies to

$$\frac{dN_{\gamma,\mathbf{q}}}{dt} = -\frac{2\pi\Omega\left|M^\gamma_{\mathbf{q}}\right|^2}{\hbar}S_0\left(\mathbf{q},\omega^\gamma_{\mathbf{q}}\right) \times \left(1 - e^{-\beta\hbar\omega^\gamma_{\mathbf{q}}}\right)\left[N_{\gamma,\mathbf{q}}(T_{\mathrm{RP}}) - N^{\mathrm{Eq}}_{\gamma,\mathbf{q}}\right],$$

where $N^{\mathrm{Eq}}_{\gamma,\mathbf{q}} = (e^{\beta\hbar\omega^\gamma_{\mathbf{q}}} - 1)^{-1}$ is the equilibrium BE distribution and $\beta = (k_B T)^{-1}$ is the inverse equilibrium thermal energy. T_{RP} here refers to the temperature of the remote phonons. Therefore, the Kapitza conductance h_{RP} of SLG coupling with the polar substrate via remote phonons is

$$h_{\mathrm{RP}} = \frac{d}{dT_{\mathrm{ph}}}\left(\frac{1}{\Omega}\sum_{\gamma,\mathbf{q}}\hbar\omega^\gamma_{\mathbf{q}}\frac{dN_{\gamma,\mathbf{q}}}{dt}\right) = -\sum_{\gamma,\mathbf{q}}\frac{2\pi\hbar\left(\omega^\gamma_{\mathbf{q}}\right)^2}{k_B T^2_{\mathrm{ph}}}\left|M^\gamma_{\mathbf{q}}\right|^2 S_0\left(\mathbf{q},\omega^\gamma_{\mathbf{q}}\right)N_{\gamma,\mathbf{q}}. \quad (2)$$

Equation (2) is used to compute h_{RP} for the different remote phonon models. The difference necessarily lies in the electron-remote phonon coupling coefficient $M^\gamma_{\mathbf{q}}$ which depends on the form of screening. It should be noted that the expression in Eq. (2) is valid for small temperature differences, applicable to the linear response heat transfer regime. If the temperature difference between the electrons and remote phonons (ΔT) is large, i.e., $T_{\mathrm{RP}} = T - \Delta T$, where T is the electron temperature, such as in pump-probe experiments[14] where laser fluences are high and ΔT can reach up to 150 K, then the rate of energy transfer from the electrons to the substrate should be calculated using the formula

$$\mathcal{J}_{\mathrm{RP}} = \frac{1}{\Omega}\sum_{\gamma,\mathbf{q}}\hbar\omega^\gamma_{\mathbf{q}}\frac{2\pi\Omega\left|M^\gamma_{\mathbf{q}}\right|^2}{\hbar}S_0\left(\mathbf{q},\omega^\gamma_{\mathbf{q}}\right)\left(1 - e^{-\beta\hbar\omega^\gamma_{\mathbf{q}}}\right) \times \left[N_{\gamma,\mathbf{q}}(T_{\mathrm{RP}} + \Delta T) - N_{\gamma,\mathbf{q}}(T_{\mathrm{RP}})\right].$$

In this paper we consider three models of RPs: unscreened surface polar phonons (u-SPP), surface polar phonons with static screening (s-SPP), and interfacial plasmon phonons (IPP). Although the theory of interfacial plasmon phonons will not be presented in this paper, some discussion of their basic elements is necessary. We plot the IPP dispersion in SiO_2-supported SLG and the electron-RP coupling coefficient for a carrier density $n = 10^{12}$ cm^{-2} in Figs. 1(a) and 1(b), respectively. In Fig. 1(a) there are three IPP and two SPP branches. The dispersion of the u-SPP and s-SPP models are the same, and are represented by the SPP branches in Fig. 1(a). We see that away from the crossing points of the plasmon and SPP branches, the IPP branches converge towards the SPP and plasmon branches in the long and short wavelength limits.

The "normalized" coupling coefficients $M^\gamma_{\mathbf{q}}(\Omega/A)^{1/2}$, where A is the area of one unit cell, for the IPP, u-SPP, and s-SPP models are shown in Fig. 1(b). The s-SPP coupling coefficient is obtained by dividing the u-SPP coefficient

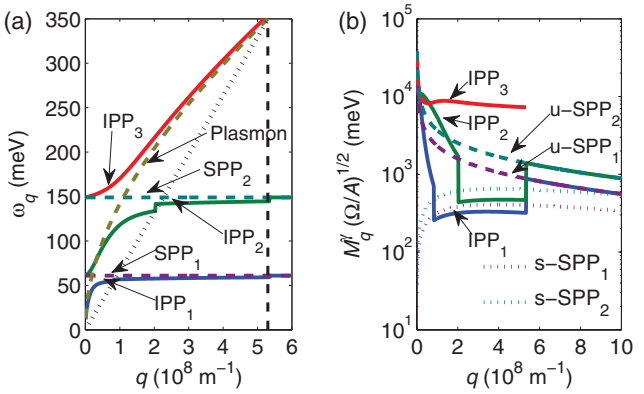

FIG. 1. (Color online) (a) Dispersion of the graphene electron (dotted line), plasmon (dashed lines), IPP (solid lines), and SPP branches (dashed lines) in the graphene-SiO_2 system at $n = 10^{12}$ cm^{-2}. The vertical dashed line represents the Landau damping cutoff q_c. (b) Corresponding plot of $M_{\mathbf{q}}^{\gamma}(\Omega/A)^{1/2}$ vs q for interfacial plasmon-phonons (IPP_1, IPP_2, and IPP_3), unscreened surface polar phonons (u-SPP_1 and u-SPP_2) and surface polar phonons with static screening (s-SPP_1 and s-SPP_2).

$M_{\mathbf{q}}^{\gamma}$ by the static dielectric function $\epsilon_{2D}(q) = 1 + \frac{q_{TF}}{q}$, in which q_{TF} is the Thomas-Fermi screening vector, i.e., $M_{\mathbf{q}}^{\gamma} \rightarrow M_{\mathbf{q}}^{\gamma}/\epsilon_{2D}(q)$. The expression for the Thomas-Fermi screening vector is $q_{TF} = e^2\Pi(q,\omega = 0)/(2\epsilon)$, where $\Pi(q,\omega = 0) = 2k_F/(\pi\hbar v_F)$ is the *static polarization* and is derived in Ref. 31, while ϵ is the average permittivity of the graphene-substrate system [$\epsilon = (\epsilon_0 + \epsilon_{ox})/2$]. This form of static screening has been used by Fratini and Guinea,[4] as well as others,[6,23,32] in modeling RP scattering. We see that as $q \rightarrow 0$, $\epsilon_{2D}(q)$ goes to infinity and the s-SPP coupling coefficient goes to zero; conversely, as $q \rightarrow \infty$, the s-SPP and u-SPP coupling coefficients converge.

Strictly speaking, it is incorrect to use static screening because RP scattering is a time-dependent perturbation which static screening does not take into account. We expect a high-frequency perturbation to be less effectively screened than a low-frequency one since the response of the screening charge in the graphene has an associated time scale. In supported SLG, the surface excitations couple to the plasmons, and this plasmon-phonon coupling modifies the scattering strength and dispersion of the surface excitations. It is from this modification of scattering strength that dynamic screening emerges and this is naturally captured in our model of interfacial plasmon phonons.[27,28] At long wavelengths ($q \rightarrow 0$) the IPP $M_{\mathbf{q}}^{\gamma}$ is stronger than $M_{\mathbf{q}}^{\gamma}$ for the s-SPP and u-SPP model. This is because when $\omega_{plasmon}(q) < \omega_{SPP}(q)$, the plasmon motion is out of phase with the bare SPP excitations, resulting in antiscreening. On the other hand, at short wavelengths ($q \rightarrow \infty$), the IPP $M_{\mathbf{q}}^{\gamma}$ is weaker because when $\omega_{plasmon}(q) > \omega_{SPP}(q)$, the screening charge can follow the motion of the SPP excitations and screening occurs. Also, like static screening, dynamic screening strength decreases with q. We also take into account the frequency dependence of the polarization as described in Ref. 28. When $\omega_{IPP}(q) > v_F q$, we use the ω-dependent polarization expression $\Pi(q,\omega) = \frac{q^2 E_F}{\pi\hbar^2\omega^2}$ to determine self-consistently the electron-IPP coupling coefficient $M_{\mathbf{q}}^{\gamma}$ and IPP dispersion $\omega_{IPP}(q)$. For each IPP branch we have a cutoff $q_c^{(\gamma)}$ determined from the equation $\omega_{IPP}^{\gamma}(q) = v_F q$. Beyond the cutoff, we switch to the ω-independent expression for the static polarization $\Pi(q) = -\frac{2E_F}{\pi\hbar^2 v_F^2}$ to determine $M_{\mathbf{q}}^{\gamma}$ and the excitation frequency for $q > q_c^{(\gamma)}$. This switching produces a discontinuity in $M_{\mathbf{q}}^{\gamma}$ and $\omega_{IPP}(q)$. This discontinuity in $M_{\mathbf{q}}^{\gamma}$ reflects the discontinuity in $\mathrm{Re}\Pi(q,\omega)$ (see Ref. 31) which affects the plasmon-SPP coupling and dynamic screening. This difference also means that interband processes are *antiscreened* while intraband processes are *screened*.

At short wavelengths, plasmons cease to be proper quasiparticles, and rapidly decay because of Landau damping. To approximate Landau damping in the IPP model, we set a cut-off wave vector q_c which is determined by the intersection of the plasmon and the graphene electron dispersion curves. When $q > q_c$, we assume that the IPP modes are Landau damped and use instead the bare SPP modes as the scattering surface excitations. Thus, the three IPP and two SPP branches couple to the graphene electrons at $q < q_c$ and $q > q_c$, respectively. This difference between the electron-IPP and electron-SPP coupling strength will be significant when we analyze the heat transfer results.

II. RESULTS AND DISCUSSION

From Eq. (2) we compute the TBC for different substrates (SiO_2, HfO_2, h-BN, and Al_2O_3) using the u-SPP, s-SPP, and IPP models. The carrier density is varied over a practical range from $n = 10^{12}$ to 10^{13} cm^{-2} over the temperature range of 50 to 400 K. The parameters for the coupling constants in Eq. (2) are taken from Refs. 5 and 33.

First, we assume the RPs to be u-SPPs. The corresponding $h_{u\text{-}SPP}$ values are plotted in Figs. 2(a) to 2(d). As we can see, $h_{u\text{-}SPP}$ increases monotonically with temperature and carrier density, and is around tens of W K^{-1} m^{-2} except in Al_2O_3 where it exceeds 100 W K^{-1} m^{-2} at room temperature. $h_{u\text{-}SPP}$ rises with carrier density because there are more electrons to scatter with the RPs. The $h_{u\text{-}SPP}$ results give us the reference case where no screening effects take place, and at this point

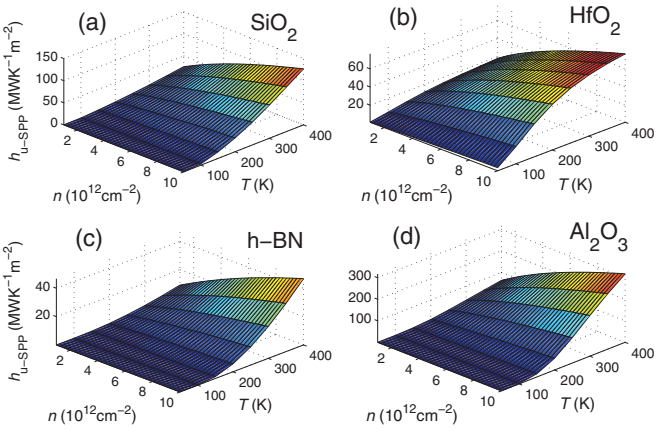

FIG. 2. (Color online) Calculated thermal conductance ($h_{u\text{-}SPP}$) between electrons in SLG and unscreened SPPs of various substrates: (a) SiO_2, (b) HfO_2, (c) h-BN, and (d) Al_2O_3 over the range $n = 10^{12}$ to 10^{13} cm^{-2} from 50 to 400 K.

we can begin to compare our results with the available experimental data. For instance, using an ultrafast optical pump pulse and monitoring the transient reflectivity on the picosecond time scale, Mak and co-workers measured the TBC of the SLG-SiO_2 interface to be around $h = 25$ MW K^{-1} m^{-2} between 300 and 400 K.[14] (Unfortunately, the carrier density in these measurements was not known.) With SiO_2, our computed $h_{u\text{-}SPP}$ is between 15 and 31 MW K^{-1} m^{-2} at $n = 10^{12}$ cm^{-2}, and between 44 and 73 MW K^{-1} m^{-2} at $n = 5 \times 10^{12}$ cm^{-2}. These values are comparable to the measured h. However, if we add the contribution from h_{ph} which is itself around 10 to 50 MW K^{-1} m^{-2},[9,13,18] then our unscreened $h_{u\text{-}SPP}$ appears too high. On the other hand, $h_{u\text{-}SPP}$ would give a good estimate of h_{RP} if plasmons were heavily damped, e.g., from electron localization,[34,35] such that they cannot couple effectively to the SO phonons.

Next, we include static screening and assume the remote phonons to be s-SPPs. The TBC $h_{s\text{-}SPP}$ values are computed, and the results are shown in Fig. 3. Compared to $h_{u\text{-}SPP}$, $h_{s\text{-}SPP}$ is about one order of magnitude smaller, which would make its experimental detection more challenging. However, $h_{s\text{-}SPP}$ still increases monotonically with respect to temperature and carrier density, although its slope with respect to carrier density is gentler because the Thomas-Fermi vector q_{TF} increases with n and the screening effect becomes stronger at higher n. Nonetheless, the greater availability of electrons to scatter with the RPs dominates thermal transport at the interface. Also, as with the u-SPP model, $h_{s\text{-}SPP}$ is the largest with the Al_2O_3 substrate, due to the large dipole coupling between Al_2O_3 and graphene.

Finally, we take the RPs to be IPPs which can be interpreted as dynamically screened SPPs. The results for the TBC h_{IPP} with various substrates are shown in Fig. 4. Quantitatively, the range of values for h_{IPP} and $h_{s\text{-}SPP}$ are comparable at low carrier densities. Again, Al_2O_3 has the largest h_{IPP}. However, we observe that h_{IPP} increases with temperature but decreases with carrier density, in stark contrast to the results in Fig. 3 where static screening was used. This carrier dependence of

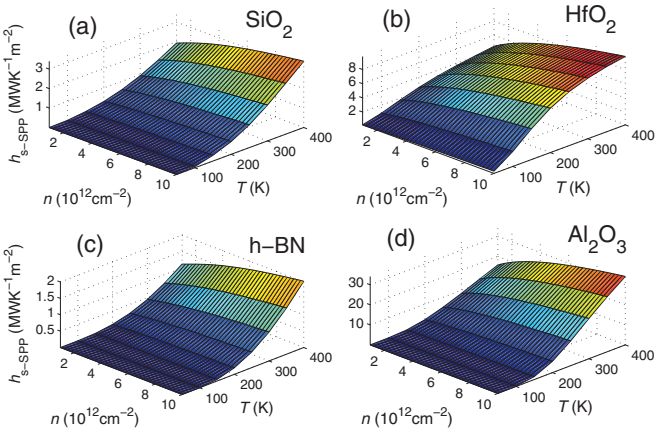

FIG. 3. (Color online) Calculated thermal conductance ($h_{s\text{-}SPP}$) between electrons in SLG and substrate SPPs with static screening. (a) SiO_2, (b) HfO_2, (c) h-BN, and (d) Al_2O_3 over the range $n = 10^{12}$ to 10^{13} cm^{-2} from 50 to 400 K. Note approximately an order of magnitude lower thermal coupling compared to the unscreened results from Fig. 2.

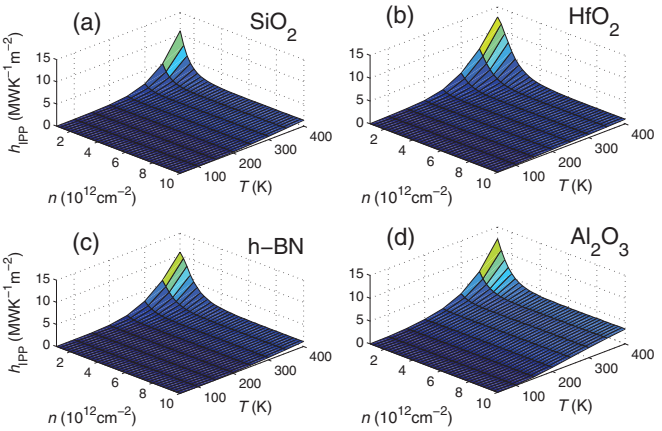

FIG. 4. (Color online) Calculated thermal conductance (h_{IPP}) between electrons in SLG and interfacial plasmon phonons (IPPs, i.e., dynamically screened SPPs) with various substrates: (a) SiO_2, (b) HfO_2, (c) h-BN, and (d) Al_2O_3 over the range $n = 10^{12}$ to 10^{13} cm^{-2} from 50 to 400 K. Note the opposite dependence on carrier density from that of Fig. 2 (unscreened SPPs) and Fig. 3 (statically screened SPPs)

h_{IPP} is counterintuitive since we expect the TBC to increase as more electrons become available for scattering. This anomaly is a consequence of electron-electron interaction that results in charge polarizability and dynamic screening. Dynamic screening depends on the frequency of the corresponding SPP and the plasmon at a given wave vector. At higher n, the plasmon frequency $\omega_{plasmon}$ increases and the plasmons can better screen the motion of RPs. In addition, more available carriers also screen the RPs. Physically, at higher carrier densities, the dielectric response of SLG becomes metal-like and the oscillating electric field from the substrate dipoles is reflected. The higher rate of energy transfer at low n is also due to the higher fraction of interband transitions, which are mediated via antiscreened IPP excitations, while at higher n, intraband transitions via screened IPP excitations are favored. In contrast, in the s-SPP model, the interband transitions can proceed through the emission and absorption of screened SPPs. Since the dielectric function $[\epsilon(q) = 1 + q_{TF}/q]$ in the s-SPP model diverges at long wavelengths, this implies that interband transitions are strongly screened. Therefore, the rate of energy transfer at small n is lower in this model. The different changes in h_{RP} at low n can also be used to verify the role of screening in interband transitions.

The striking contrast between the carrier density dependence of h_{IPP} and $h_{s\text{-}SPP}$ highlights the difference between the different models of screening and could be readily detected in experimental measurements of thermal boundary resistance in supported SLG.[11,14] We plot h_{IPP}, $h_{s\text{-}SPP}$, and $h_{u\text{-}SPP}$ at room temperature (300 K) in Fig. 5 for all four substrates investigated here. We see that of the four dielectrics, Al_2O_3 seems to offer the best prospect for verifying the effects of dynamic screening in interfacial thermal transport. Ideally, the experiment should be performed at around a carrier density 10^{12} cm^{-2} between 300 and 400 K on Al_2O_3-supported SLG. By modulating a gating voltage and varying n from 10^{12} to 5×10^{12} cm^{-2}, a change in h of the order of magnitude of $\sim$10 MW K^{-1} m^{-2} should be detectable in the s-SPP

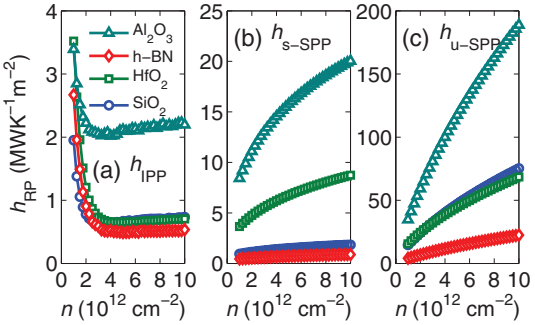

FIG. 5. (Color online) Comparison of the three different models of thermal coupling (hRP) between graphene electrons and remote substrate phonons considered in this paper, over the range $n = 10^{12}$ to 10^{13} cm^{-2} at 300 K. (a) h_{IPP} for interfacial plasmon phonons, (b) $h_{s\text{-}SPP}$ for statically screened SPPs, and (c) $h_{u\text{-}SPP}$ for unscreened SPPs. The four plotted sets correspond to SiO_2, HfO_2, h-BN, and Al_2O_3 substrates. Note the different y-axis scales.

model. In the IPP model, one should see a decrease of $\sim$1 MW K^{-1} m^{-2}. These variations would be observed superimposed to the phonon-phonon contribution to the TBC ($h_{ph} \sim$ 10 to 50 MW K^{-1} m^{-2}), as long as the SLG samples are of sufficiently high quality such that the plasmons are not damped too much by defects.

However, there is one possible complication from the application of a bottom gate voltage, which is known to exert an electrostatic force in the direction normal to the graphene-SiO_2 direction.[36,37] Thus, as the bottom gate voltage is increased, the carrier density within the graphene as well as the electrostatic force pulling the graphene towards the membrane increases. The increase in the electrostatic force at the interface may result in an increase in the phonon contribution to interfacial thermal transport.[15] Hence, the decrease in h with n as predicted by the IPP model may be at least partially canceled out by the increase in h from the larger electrostatic force.

III. CONCLUSION

We have calculated the thermal boundary conductance for single-layer graphene supported by various substrates, using models of surface excitations with different types of remote phonon screening. The TBC temperature and carrier density dependence have been determined. We find that the difference between static and dynamic screening is manifested in the carrier dependence of the TBC. An experiment measuring the difference is proposed using Al_2O_3-supported, high-quality SLG.

ACKNOWLEDGMENTS

A.Y.S. and E.P. acknowledge funding from the National Science Foundation (NSF) CAREER award 09-54423 and from the Nanotechnology Research Initiative (NRI). Z.-Y.O. and M.V.F. acknowledge support from Texas Instruments, the Semiconductor Research Corporation, the Microelectronics Advanced Research Corporation, the Focus Center Research Project for Materials, Structure and Devices (MSD) and Samsung Electronics Ltd.

*zhunyong.ong@utdallas.edu
†epop@illinois.edu

[1] V. E. Dorgan, M.-H. Bae, and E. Pop, Appl. Phys. Lett. **97**, 082112 (2010).
[2] E. V. Castro, H. Ochoa, M. I. Katsnelson, R. V. Gorbachev, D. C. Elias, K. S. Novoselov, A. K. Geim, and F. Guinea, Phys. Rev. Lett. **105**, 266601 (2010).
[3] V. E. Dorgan, A. Behnam, H. J. Conley, K. I. Bolotin, and E. Pop, Nano Lett. (2013), doi:10.1021/nl400197w.
[4] S. Fratini and F. Guinea, Phys. Rev. B **77**, 195415 (2008).
[5] V. Perebeinos and P. Avouris, Phys. Rev. B **81**, 195442 (2010).
[6] A. Konar, T. Fang, and D. Jena, Phys. Rev. B **82**, 115452 (2010).
[7] M. H. Bae, S. Islam, V. E. Dorgan, and E. Pop, ACS Nano **5**, 7936 (2011).
[8] S. Islam, Z. Li, V. Dorgan, M.-H. Bae, and E. Pop, IEEE Electron Device Lett. **34**, 166 (2013).
[9] E. Pop, Nano Res. **3**, 147 (2010).
[10] Y. Lin, K. Jenkins, A. Valdes-Garcia, J. Small, D. Farmer, and P. Avouris, Nano Lett. **9**, 422 (2008).
[11] Y. K. Koh, M. H. Bae, D. G. Cahill, and E. Pop, Nano Lett. **10**, 4363 (2010).
[12] B. Persson and H. Ueba, Europhys. Lett. **91**, 56001 (2010).
[13] Z.-Y. Ong and E. Pop, Phys. Rev. B **81**, 155408 (2010).
[14] K. Mak, C. Lui, and T. Heinz, Appl. Phys. Lett. **97**, 221904 (2010).
[15] W. Hsieh, A. Lyons, E. Pop, P. Keblinski, and D. Cahill, Phys. Rev. B **84**, 184107 (2011).
[16] Z. Chen, W. Jang, W. Bao, C. Lau, and C. Dames, Appl. Phys. Lett. **95**, 161910 (2009).
[17] H. Lyeo and D. Cahill, Phys. Rev. B **73**, 144301 (2006).
[18] Z.-Y. Ong and E. Pop, J. Appl. Phys. **108**, 103502 (2010).
[19] Z.-Y. Ong, E. Pop, and J. Shiomi, Phys. Rev. B **84**, 165418 (2011).
[20] S. Rotkin, V. Perebeinos, A. Petrov, and P. Avouris, Nano Lett. **9**, 1850 (2009).
[21] S. Wang and G. Mahan, Phys. Rev. B **6**, 4517 (1972).
[22] V. Perebeinos, S. Rotkin, A. Petrov, and P. Avouris, Nano Lett. **9**, 312 (2008).
[23] T. Low, V. Perebeinos, R. Kim, M. Freitag, and P. Avouris, Phys. Rev. B **86**, 045413 (2012).
[24] J. Viljas and T. Heikkilä, Phys. Rev. B **81**, 245404 (2010).
[25] Z. Fei, G. Andreev, W. Bao, L. Zhang, A. S. McLeod, C. Wang, M. Stewart, Z. Zhao, G. Dominguez, M. Thiemens *et al.*, Nano Lett. **11**, 4701 (2011).
[26] Y. Liu and R. F. Willis, Phys. Rev. B **81**, 081406 (2010).
[27] Z.-Y. Ong and M. V. Fischetti, Phys. Rev. B **86**, 165422 (2012).
[28] Z.-Y. Ong and M. V. Fischetti, Phys. Rev. B **86**, 199904 (2012).
[29] P. Phillips, *Advanced Solid State Physics* (Cambridge University Press, Cambridge, 2012).
[30] E. H. Hwang and S. Das Sarma, Phys. Rev. B **75**, 205418 (2007).
[31] B. Wunsch, T. Stauber, F. Sols, and F. Guinea, New J. Phys. **8**, 318 (2006).
[32] X. Li, E. Barry, J. Zavada, M. Nardelli, and K. Kim, Appl. Phys. Lett. **97**, 232105 (2010).

[33]M. V. Fischetti, D. A. Neumayer, and E. A. Cartier, J. Appl. Phys. **90**, 4587 (2001).
[34]S. Lamba and D. Kumar, Phys. Rev. B **59**, 4766 (1999).
[35]J. H. Davies, P. A. Lee, and T. M. Rice, Phys. Rev. B **29**, 4260 (1984).
[36]W. Bao, K. Myhro, Z. Zhao, Z. Chen, W. Jang, L. Jing, F. Miao, H. Zhang, C. Dames, and C. N. Lau, Nano Lett. **12**, 5470 (2012).
[37]N. Lindahl, D. Midtvedt, J. Svensson, O. A. Nerushev, N. Lindvall, A. Isacsson, and E. E. B. Campbell, Nano Lett. **12**, 3526 (2012).